ACS APPLIED MATERIALS & INTERFACES

Research Article

www.acsami.org

Colloidal $CuInS_2$ Quantum Dots as Inorganic Hole-Transporting Material in Perovskite Solar Cells

Mei Lv,[†] Jun Zhu,*[,†] Yang Huang,[†] Yi Li,[†] Zhipeng Shao,[†] Yafeng Xu,[†] and Songyuan Dai*[,†,‡]

[†]Key Laboratory of Novel Thin Film Solar Cells, Hefei Institutes of Physical Science, Chinese Academy of Sciences, Hefei 230031, P. R. China

[‡]Beijing Key Laboratory of Novel Thin Film Solar Cells, State Key Laboratory of Alternate Electrical Power System with Renewable Energy Sources, North China Electric Power University, Beijing 102206, P. R. China

ABSTRACT: To develop novel hole-transporting materials (HTMs) is an important issue of perovskite solar cells (PSCs), especially favoring the stability improvement and the cost reduction. Herein, we use ternary quantum dots (QDs) as HTM in mesoporous $TiO_2/CH_3NH_3PbI_3$/HTM/Au solar cell, and modify the surface of $CuInS_2$ QDs by cation exchange to improve the carrier transport. The device efficiency using $CuInS_2$ QDs with a ZnS shell layer as HTM is 8.38% under AM 1.5, 100 mW cm^{-2}. The electrochemical impedance spectroscopy suggested that the significantly enhanced performance is mainly attributed to the reduced charge recombination between TiO_2 and HTM. It paves a new pathway for the future development of cheap inorganic HTMs for the high efficiency PSCs.

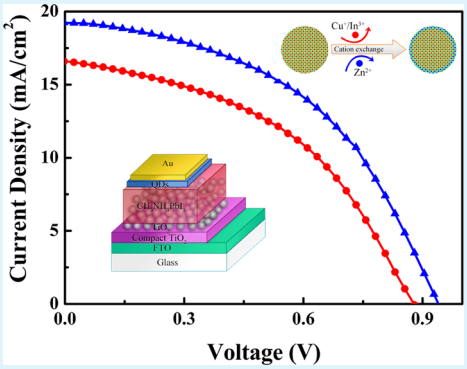

KEYWORDS: *$CuInS_2$, quantum dots, hole-transporting materials, perovskite solar cells, interface recombination*

INTRODUCTION

Methylammonium lead halide ($CH_3NH_3PbX_3$, X = I, Cl, or Br) and its mixed-halide crystals have been used as both light absorber and charge transporter for a novel type of revolutionary solar cell.[1−3] The advantages of $CH_3NH_3PbX_3$ crystals are the direct band gap, large absorption coefficient, and high carrier mobility,[4−6] which render them to be flawless light harvesters and ambipolar transporter.[7−9] Most recently, a certified power conversion efficiency (PCE) over 20% has been obtained,[10] which is comparable to that of the commercial silicon solar cells. PSCs generally employ organic HTMs such as Spiro-OMeTAD,[11] PTAA,[12] P3HT,[13] PANI,[14] and so on. However, the cost is increasing to employ these HTMs in PSCs because the synthetic methods are complicated and high purity is needed for photovoltaic applications. For example, the current commercial price of high-quality Spiro-OMeTAD is over \$600 g^{-1}, which is many times more than precious metal. It limits the further large-scale application of cost-effective PSCs.

Some inorganic HTMs have already been proved in PSCs in previous reports such as CuSCN,[15] CuI,[16] and PbS.[17−19] There are many distinctive properties of quantum dots (QDs) when being employed in photovoltaics such as tunable bandgap,[20] inherently high absorption coefficient,[21] hot electron transfer,[22] and multiple exciton generation.[23] In this paper, we report on "green" inorganic HTMs replacing the organic hole conductor, demonstrating an inexpensive, solution-processable, inorganic HTM for the PSCs. Ternary semiconductor copper indium disulfide ($CuInS_2$) is a less toxic alternative to cadmium- or lead-containing semiconductors with a direct bandgap in the bulk of 1.45 eV and Bohr exciton radius of 4.1 nm.[24] It has favorable features such as a high extinction coefficient in the visible spectral range,[25] proper band gap well-matched to the solar spectrum,[26] exceptional radiation hardness, and pronounced defect tolerance.[24] $CuInS_2$ QDs have been demonstrated with the new record efficiency in liquid quantum dot-sensitized solar cells (QDSSCs).[27] Herein, $CuInS_2$ is selected on the basis of its suitable valence band position, p-type conductivity,[28−30] and the compatibility of the solution deposition method with the organic-lead halide perovskite absorber. Modifying the surface of $CuInS_2$ QDs by cation exchange is employed to improve the charge transport and therefore the device performance. We have achieved a PCE of 8.38% for the PSC employing modified $CuInS_2$ QDs as HTM.

EXPERIMENTAL SECTION

Materials. Indium acetate ($In(OAc)_3$, 99.99%), oleylamine (OAm, 97%), 1-octadecene (ODE, 90%), sulfur powder (S, 99.99%), lead(II) iodide (PbI_2, 99%), 4-*tert*-butylpyridine (tBP, 96%), titanium(IV) isopropoxide (TTIP, 97%), lithium bis(trifluoromethylsulfonyl) imide (Li-TFSI, 99.95%), and N,N-dimethylformamide (DMF) were purchased from Aldrich. Copper iodide (CuI, 99.998%) and diethyl ether (99%) were obtained from Alfa Aesar, while Spiro-OMeTAD (purity. 99.5%) was purchased from Merck KGaA. All chemicals were used as received without further processing. Patterned FTO coated

Received: June 11, 2015
Accepted: July 17, 2015
Published: July 17, 2015

DOI: 10.1021/acsami.5b05104
ACS Appl. Mater. Interfaces 2015, 7, 17482−17488

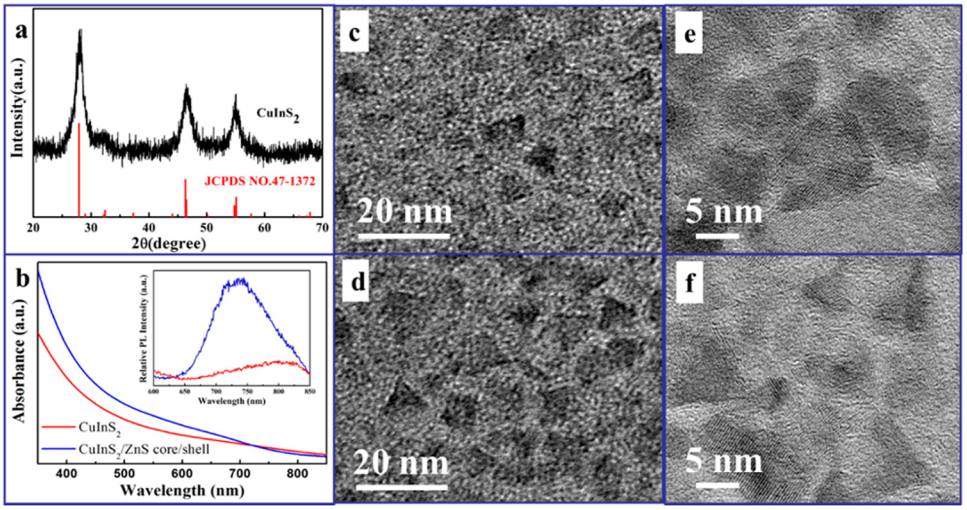

Figure 1. (a) XRD pattern of the as-synthesized $CuInS_2$ QD, (b) UV−vis absorption and fluorescence spectra of the as-synthesized $CuInS_2$ and $CuInS_2$/ZnS core/shell QDs; (c) TEM image and (e) HRTEM micrograph of the as-synthesized $CuInS_2$ QD; (d) TEM image and (f) HRTEM micrograph of the $CuInS_2$/ZnS core/shell QDs.

glass substrates with a sheet resistance of 15 $\Omega \cdot sq^{-1}$ were supplied from TEC company.

Synthesis of $CuInS_2$ QDs. We synthesize $CuInS_2$ QDs using the method reported by Zhong et al.[27] Typically, 0.1 mmol of CuI and 0.1 mmol of $In(OAc)_3$ were added to 2.0 mL of OAm and 4.0 mL of ODE and degassed at 40 °C for 20 min in a 50 mL flask. Subsequently, the mixture solution was heated to 180 °C under argon flow, and once it reached 180 °C, 0.4 mmol of sulfur dissolved in 0.4 mL of OAm was injected into the reaction system for the QDs nucleation growth 20 min. The purified $CuInS_2$ QDs were obtained by precipitation and centrifugation procedure. Then, they were dispersed in *n*-hexane for use in the next step. The shell precursors $Zn(OAc)_2$ solution was injected into the reaction system of as synthesized $CuInS_2$ nanocrystals at about 100 °C and kept at this temperature for 30 min to employ the cation exchange procedure for the growth of the shell material.

Device Fabrication. FTO-coated glass substrate with high transparency in the visible range with dimension of 2 cm × 1.5 cm was patterned by etching with Zn powder and 2 M HCl diluted in water. The etched substrate was cleaned with detergent, rinsed with deionized water and ethanol in an ultrasonic bath for 30 min, and then dried by air. Finally, the substrate was annealed at 500 °C for 30 min.

A TiO_2 compact layer was then deposited on the cleaned transparent conducting oxide substrates by spin-coating a mildly acidic solution of TTIP at 2000 rpm for 30 s according to a reported method,[8] and then annealed at 500 °C for 30 min.

A mesoporous TiO_2 layer composed of commercial TiO_2 paste (Dyesol18NRT, Dyesol) diluted in ethanol (1:3.5, weight ratio) was then deposited on the top of compact layer by spin-coating at 5000 rpm for 30 s. After drying at 125 °C, the TiO_2 films were annealed at 500 °C for 30 min to remove the organic matter. After cooling to room temperature naturally, the TiO_2 films were treated in a 0.04 M aqueous solution of $TiCl_4$ at 70 °C for 30 min, rinsed with deionized water and following annealed at 500 °C for 30 min.

PbI_2 powder was dissolved in DMF at a concentration of 462 mg mL^{-1} (1 M) under stirring at 70 °C followed by filtering with a PVDF syringe filter (0.22 μm). The solution was kept at 70 °C during the whole procedure. 40 μL PbI_2 solution was spin-coated on the mesoporous TiO_2 films at 3000 rpm for 20 s, and dried at 50 °C for 3 min and 100 °C for 5 min consecutively. After cooling down, 100 μL CH_3NH_3I solution in 2-propanol (10 mg mL^{-1}) was loaded on the PbI_2-coated TiO_2 films for 20 s, which was spun at 4000 rpm for 30 s and then dried at 100 °C for 5 min.

The HTMs were deposited on the $CH_3NH_3PbI_3$-coated TiO_2 films by spin-coating at 4000 rpm for 30 s, which is a solution of 72.3 mg Spiro-OMeTAD, 28.8 μL TBA, 17.5 μL of a solution of 520 mg mL^{-1} LiTFSI in acetonitrile in 1 mL of chlorobenzene. The inorganic HTMs colloidal $CuInS_2$ QDs or $CuInS_2$/ZnS core/shell QDs (about 5 mg mL^{-1}) with their original ligands (oleylamine) were deposited by spin-coating on top of the $CH_3NH_3PbI_3$-coated TiO_2 films at 4000 rpm for 30 s.

Finally, 60 nm thick gold was thermally evaporated on top of the device to form the back contact. The active area of devices were 9 mm^2 determined by a black mask with dimension of 3 mm × 3 mm.

Characterization. The crystallinity of QDs was determined using X-ray powder diffraction analysis (XRD, TTR-III, Rigaku Corp., Japan) with Cu−Kα irradiation (λ = 1.5406 Å). The cross-sectional morphologies of the photoelectrodes were investigated by a field emission scanning electron microscopy (FE-SEM, sirion200, FEI Corp., Holland). The TEM images were observed with transmission electron microscopy (TEM, JEOL-2010, Japan). The UV−vis spectrum of the films was obtained using a UV−vis spectrophotometer (U-3900H, HITACHI, Japan). The current−voltage characteristics (*J*−*V*) measurements were carried out on a Keithley model 2420 digital source meter controlled (Keithley Instruments, Inc., OH) by test point software under a xenon lamp (100 mW cm^{-2}) provided by a solar simulator (solar AAA simulator, Oriel USA). The IPCE measurementwas conducted using a QE/IPCE measurement kit (Newport Corporation, USA). The electrochemical impedance spectra (EIS) were recorded by a computer controlled potentiostat (Autolab 320, Metrohm, Switzerland) in a frequency range of 1 Hz ∼ 1 MHz applied in the dark. The obtained impedance spectra were fitted with ZView software (v2.8b, Scribner Associates, USA).

RESULTS AND DISCUSSION

Characteristics of $CuInS_2$ and $CuInS_2$/ZnS Core/Shell QDs. Figure 1a shows the X-ray diffraction (XRD) spectrum of the $CuInS_2$ QDs. The diffraction peaks are identified as the tetragonal chalcopyrite structure according to JCPDS 47−1372 data. An intense peak at 2θ = 27.4° corresponds to the (112) crystal plane. Other prominent peaks correspond to the (204)/(220), (116)/(312), and (004)/(200) planes. In addition to these commonly observed orientations, the weak peaks such as (103) and (301) are also observed in the XRD pattern, distinguishing the chalcopyrite phase from the sphalerite phase. To passivate the surface defect, a ZnS layer was over coated around the presynthesized $CuInS_2$ QDs to form the $CuInS_2$/ZnS core/shell heterostructure QDs via cation exchange.[27] Figure 1b shows the absorption spectra and fluorescence spectra of $CuInS_2$ and $CuInS_2$/ZnS core/shell QDs in normal

DOI: 10.1021/acsami.5b05104
ACS Appl. Mater. Interfaces 2015, 7, 17482−17488

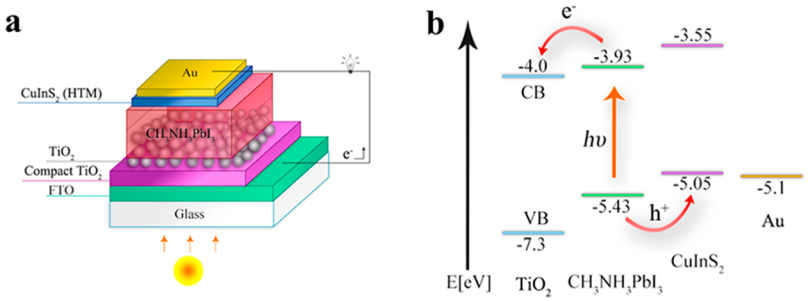

Figure 2. Device architecture and energy level diagram. (a) Schematics view of the perovskite solar cell configuration: FTO glass, compact TiO_2 under layer, mesoporous TiO_2 with infiltrated $CH_3NH_3PbI_3$, $CuInS_2$ HTM, and gold. (b) Energy level diagram of the $TiO_2/CH_3NH_3PbI_3/CuInS_2$/Au device showing electron injection and hole extraction.

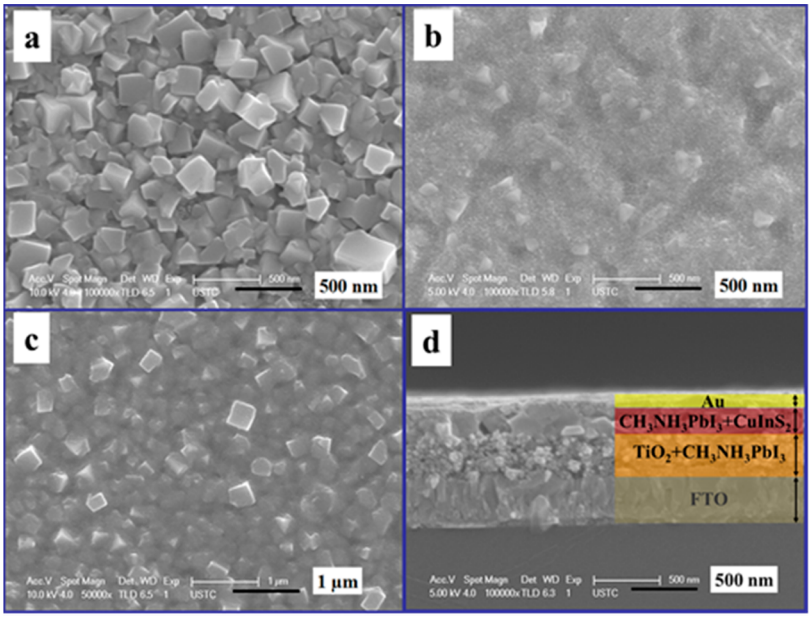

Figure 3. Top view SEM image of (a) $CH_3NH_3PbI_3$, (b) $CH_3NH_3PbI_3/CuInS_2$ QD, and (c) $CH_3NH_3PbI_3/CuInS_2$/ZnS core/shell heterostructure QDs deposited on the surface of TiO_2 films; (d) cross-sectional SEM structure of complete typical perovskite $CH_3NH_3PbI_3$ device.

hexane solvent. These QDs display a broad characteristic shoulder, which fail to emerge sharp excitonic peaks as PbS[31] or CdSe.[32] The main reason is that the dominance of internal and surface defects as previous studies reported.[20,33,34] The overgrowth with ZnS typically leads to a blue shift of the PL spectrum (Figure 1b inset), which is likely indicative of etching of the core size under a thin shell growth conditions and the associated increase in the degree of spatial confinement.[33] The use of wide band gap ZnS over coating results in a dramatic improvement of the PL quantum yield. According to previous reports, the cation exchange method makes the native core QD transfer into core/shell heterostructure QD without enhancing the particle size and changing the particle shape due to the absence of counteranion.[27,35] This is verified by the TEM image (Figure 1e, f) of the QDs with triangle shape and size around 4 nm in diameter.[20] Moreover, the wide-field TEM images (Figure 1c, d) show that the resulting QDs have a narrow size distribution.

$TiO_2/CH_3NH_3PbI_3$/QDs/Au Solar Cells. The sequential deposition technique was used to fabricate the mesoscopic PSCs employing the $CuInS_2$ QDs and $CuInS_2$/ZnS QDs as HTMs.[36] Currently, mesoporous TiO_2 scaffold layer is generally utilized as a porous substrate on which the $CH_3NH_3PbI_3$ light absorber can be deposited. In addition to acting as a scaffold layer, the mesoporous TiO_2 film is responsible for accepting electrons from the absorber and transporting them to the FTO substrate.[36,37] Besides, the compact TiO_2 hole-blocking layer is needed to keep holes formed in the perovskite or HTM layer from reaching the FTO electrode, as this would make the cell short-circuited.[38,39] The device's configuration is shown in Figure 2a. We plotted the energy level diagram of the materials used in our devices in Figure 2b according to the positions of the conduction bandedge (CB) and valence bandedge (VB) of the $CuInS_2$ QDs.[40] We note there are literature reports providing different values. Actually, the exact values of the energy levels depend on the measurement and the QD synthetic methodology. The VB of the $CuInS_2$ QDs (−5.05 eV) in our study is perfect compared to the VB of $CH_3NH_3PbI_3$ (−5.43 eV), which favors hole from $CH_3NH_3PbI_3$ transfer into the inorganic HTM. It is worth remarking that the VB value of the $CuInS_2$ QDs in the literature reports have a broad distribution. The inherent energetic disorder of the $CuInS_2$ QDs broadens the shape of its VB, which enabling the hole injection process. Figure 3a shows a scanning electron microscope top view image of the perovskite film on the TiO_2 film in which the crystal domains of the $CH_3NH_3PbI_3$ can be observed. It indicates the presence of perovskite crystals on top of the TiO_2 film. The treated film

DOI: 10.1021/acsami.5b05104
ACS Appl. Mater. Interfaces 2015, 7, 17482−17488

highlights the formation of $CH_3NH_3PbI_3$ in crystals ranging from tens of nanometers to hundreds of nanometers in size from Figure 3a as that generally reported.[41] The HTMs are subsequently deposited by spin-coating. After annealing, the $CuInS_2$ QDs or $CuInS_2$/ZnS core/shell QDs HTM was spin-coated on the $TiO_2/CH_3NH_3PI_3$ film. The QDs penetrate into the remaining available $CH_3NH_3PbI_3$ pore volume and form a capping layer on top of the composite structure, which can be observed in Figure 3b ($CuInS_2$ QDs) and Figure 3c ($CuInS_2$/ZnS core/shell QDs). Figure 3d shows a cross-sectional SEM picture. Because the $CH_3NH_3PbI_3$ will degrade in the presence of polar solvent, the generally employed layer-by-layer method for QD films does not work here and we just spin-coat the QD solution once. The QD layer thickness is in the range of tens of nanometers from the SEM image, smoothing the perovskite crystal cuboids surface. A thin gold layer is thermally evaporated under vacuum onto the HTMs, forming the back contact of the device. The transmittance of the $TiO_2/CH_3NH_3PbI_3$ films before and after spin-coating the QDs are shown in Figure 4. The transmittance of the $TiO_2/CH_3NH_3PbI_3$ film is significantly increased within the range 550−800 nm comparing with that within the shorter wavelength region, similar as previously report about the absorption spectra of perovskite.[18] However, the transmittance of the film is slightly increased after spin-coating the colloidal QDs. The reasons are that the light scattering of $CH_3NH_3PbI_3$ cuboids is reduced due to the solvent effect during the spin-coating procedure and the QD layer absorption is negligible due to its thickness. The transmittance of $TiO_2/CH_3NH_3PbI_3/CuInS_2$/ZnS core/shell film is even higher than $TiO_2/CH_3NH_3PbI_3/CuInS_2$ film and its effect on the device performance such as short circuit current will be discussed later.

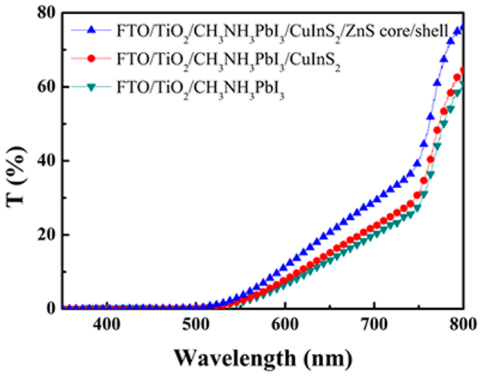

Figure 4. Transmittance spectra of $TiO_2/CH_3NH_3PbI_3$ film before and after spinning quantum dots.

Photovoltaic Performance. To demonstrate the potential of $CuInS_2$ QDs in PSCs, we compared the devices with the common Spiro-OMeTAD as HTM and without HTMs were prepared and the efficiencies. Figure 5a shows the $J-V$ curves of the PSCs employed QDs as HTMs. The photovoltaic parameters of the PSCs are summarized in Table 1. A PCE of 5.28% was achieved for the hole conductor-free device, lower than Etgar's reported,[7] where $CH_3NH_3PbI_3$ film formation was induced by spin-coating $CH_3NH_3PbI_3$ film twice. Here, we follow the sequential $CH_3NH_3PbI_3$ film method, where the PbI_2 film layer is spin-coated only once, for the $TiO_2/CH_3NH_3PbI_3$/QDs/Au cell with the optimized efficiency. The $TiO_2/CH_3NH_3PbI_3/CuInS_2$/Au cell gives a J_{sc} of 16.6 mA cm^{-2}, a V_{oc} of 0.878 V, and a FF of 45.1% reaching a PCE of 6.57%. Both J_{sc} and V_{oc} are improved compared with device free of HTMs, although the FF is decreased, leading to an increased efficiency. To further improve the device efficiency, the surface of $CuInS_2$ QDs was passivated. The surface traps of QDs usually play a key role for the device performance and there have been many reports on the surface passivation effect on QD solar cell efficiency. Alivisatos et al. first reported the synthesis of core/shell heterostructure via cation exchange.[35] This strategy shows a beneficial effect on the photoluminescence properties of the cores due to the decreasing of the defect density. We synthesize the $CuInS_2$/ZnS core/shell QDs and use them as HTMs for PSCs. After the QD surface modification, the PSC efficiency was remarkably increased. The $TiO_2/CH_3NH_3PbI_3/CuInS_2$/ZnS/Au cell gives a J_{sc} of 18.6 mA cm^{-2}, a FF of 48.7%, and a V_{oc} of 0.924 V reaching an impressive PCE of 8.38%. The performance improvement was attributed to core/shell heterostructure. Compared with the common Spiro-OMeTAD as HTMs, the PCE is still low

Table 1. Photovoltaic Characteristics of PSCs

cell	J_{sc} (mA/cm^2)[a]	V_{oc} (V)[b]	FF (%)[c]	PCE (%)[d]
$TiO_2/CH_3NH_3PbI_3$/Spiro-OMeTAD/Au	19.7	1.02	69.3	13.9
$TiO_2/CH_3NH_3PbI_3/CuInS_2$/Au	16.6	0.878	45.1	6.57
$TiO_2/CH_3NH_3PbI_3/CuInS_2$/ZnS/Au	18.6	0.924	48.7	8.38
$TiO_2/CH_3NH_3PbI_3$/Au	12.6	0.797	56.5	5.66

[a]Open-circuit photovoltage. [b]Short-circuit photocurrent. [c]Fill factor. [d]Power conversion efficiency.

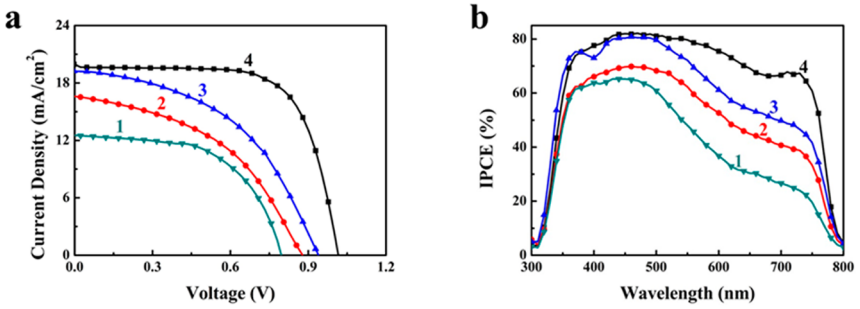

Figure 5. (a) $J-V$ curves and (b) IPCE curves of PSCs: (1) $TiO_2/CH_3NH_3PbI_3$/Au cell, (2) $TiO_2/CH_3NH_3PbI_3/CuInS_2$/Au cell, (3) $TiO_2/CH_3NH_3PbI_3/CuInS_2$/ZnS/Au cell, (4) $TiO_2/CH_3NH_3PbI_3$/Spiro-OMeTAD/Au cell.

DOI: 10.1021/acsami.5b05104
ACS Appl. Mater. Interfaces 2015, 7, 17482−17488

(8.38% vs 13.9%) and there is much room for FF improvement (45.1% vs 69.3%). The organic ligands on the QD surface may be one reason for the lower FF and it may be optimized by using shorter linker molecules. Because of the smaller thickness of the QD layer compared with that of the Spiro-OMeTAD layer, we believe increasing the QD layer thickness and improving the hole transport will increase the shunt resistance and therefore improve the FF. The incident photon to current efficiency (IPCE) or external quantum efficiency (EQE) spectra represent the ratio of extracted electrons to incident photons at the electrode surface at a given wavelength. The corresponding IPCE spectra of the devices with various HTMs are plotted in Figure 5b. Compared with the PSC free of HTM, the IPCE spectrum of $TiO_2/CH_3NH_3PbI_3/CuInS_2/Au$ cell is significantly improved in the range of 400−800 nm, more pronounced in the longer wavelength. Because of the introduction of $CuInS_2$ QD layer into the device does not lead to noticeable absorption change, the increased spectral response should be attributed to the improved charge collection in the presence of QD HTM. The IPCE result is further enhanced in all the measured wavelength range after the $CuInS_2$ QD is passivated with ZnS shell layer. There is still room for the improvement of IPCE if we compare it with that of $TiO_2/CH_3NH_3PbI_3$/Spiro-OMeTAD/Au cell. Increasing the light scattering using bigger TiO_2 nanoparticles or submicrospheres should resolve the problem. Integration of the IPCE spectra gives a J_{sc} of 18 mA cm^{-2}, which is in good agreement with the current density from the $J-V$ measurements.

Electrochemical Impedance Spectroscopy. Electrochemical impedance spectroscopy (EIS) can intuitively describe the recombination processes in PSCs,[42−44] and the recombination resistance (R_{rec}) can be obtained by fitting the impedance spectra with appropriate equivalent circuit. The first arc at high frequency is related to the hole transport and extraction between the HTM and cathode.[42,45] The main arc at middle freuency is due to the recombination between TiO_2 and HTMs.[16,43] The solar cells with $CuInS_2$ and $CuInS_2$/ZnS core/shell QDs as HTM were analyzed at foreword bias of 0.8 V under dark conditions. The obtained spectra (Figure 6) present the main arc at middle freuency range of 0.4 kHz to 50 kHz. There is some disorder in the low frequency data, which is common phenomenon in the PSCs.[46−48] R_{rec} for $TiO_2/CH_3NH_3PbI_3/CuInS_2/ZnS/Au$ cell shows larger value than that for $TiO_2/CH_3NH_3PbI_3/CuInS_2/Au$ cell, which indicates that recombination in the device based on $CuInS_2$/ZnS core/shell QDs is slower compared to $CuInS_2$-based devices, a reasonable interpretation for the improved efficiency. The retarded recombination is due to the decrease in the surface trap density in core/shell QDs.

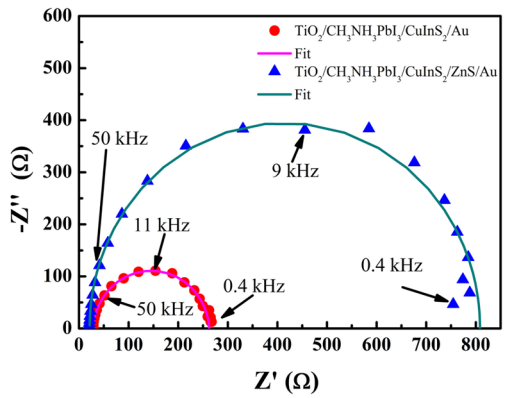

Figure 6. Nyquist plots for the perovskite solar cells with $CuInS_2$ and $CuInS_2$/ZnS as HTM, measured under dark conditions at 0.8 V bias.

CONCLUSION

In summary, we have demonstrated the $CuInS_2$ QDs as inorganic hole conductor for efficient PSCs by a solution process. Modifying the surface of $CuInS_2$ QDs by cation exchange to form $CuInS_2$/ZnS core/shell heterostructure QDs and using them as HTMs give a PCE of 8.38%. Unmodified $CuInS_2$ QDs as HTM provides PCE lower than $CuInS_2$/ZnS core/shell QDs because of higher recombination between TiO_2 and HTM indicated by the electrochemical impedance spectroscopy results.

AUTHOR INFORMATION

Corresponding Authors

*E-mail: zhujzhu@gmail.com. Tel: +86 0551-65592190.
*E-mail: sydai@ipp.ac.cn. Tel: +86 0551-65591377.

Notes

The authors declare no competing financial interest.

ACKNOWLEDGMENTS

The research described herein was supported by the National Basic Research Program of China under Grant 2011CBA00700, and the National Natural Science Foundation of China under Grants 21403247 and 61204075.

REFERENCES

(1) Kojima, A.; Teshima, K.; Shirai, Y.; Miyasaka, T. Organometal Halide Perovskites as Visible-Light Sensitizers for Photovoltaic Cells. *J. Am. Chem. Soc.* **2009**, *131*, 6050−6051.
(2) Im, J. H.; Lee, C. R.; Lee, J. W.; Park, S. W.; Park, N. G. 6.5% Efficient Perovskite Quantum-Dot-Sensitized Solar Cell. *Nanoscale* **2011**, *3*, 4088−4093.
(3) Kim, H. S.; Lee, C. R.; Im, J. H.; Lee, K. B.; Moehl, T.; Marchioro, A.; Moon, S. J.; Humphry-Baker, R.; Yum, J. H.; Moser, J. E.; Gratzel, M.; Park, N. G. Lead Iodide Perovskite Sensitized All-Solid-State Submicron Thin Film Mesoscopic Solar Cell with Efficiency Exceeding 9%. *Sci. Rep.* **2012**, *2* (591), 1−7.
(4) Kojima, A.; Ikegami, M.; Teshima, K.; Miyasaka, T. Highly Luminescent Lead Bromide Perovskite Nanoparticles Synthesized with Porous Alumina Media. *Chem. Lett.* **2012**, *41*, 397−399.
(5) Kagan, C. R.; Mitzi, D. B.; Dimitrakopoulos, C. D. Organic-inorganic Hybrid Materials as Semiconducting Channels in Thin-Film Field-Effect Transistors. *Science* **1999**, *286*, 945−947.
(6) Wehrenfennig, C.; Eperon, G. E.; Johnston, M. B.; Snaith, H. J.; Herz, L. M. High Charge Carrier Mobilities and Lifetimes in Organolead Trihalide Perovskites. *Adv. Mater.* **2014**, *26*, 1584−1589.
(7) Laban, W. A.; Etgar, L. Depleted Hole Conductor-Free Lead Halide Iodide Heterojunction Solar Cells. *Energy Environ. Sci.* **2013**, *6*, 3249−3253.
(8) Eperon, G. E.; Stranks, S. D.; Menelaou, C.; Johnston, M. B.; Herz, L. M.; Snaith, H. J. Formamidinium Lead Trihalide: A Broadly Tunable Perovskite for Efficient Planar Heterojunction Solar Cells. *Energy Environ. Sci.* **2014**, *7*, 982−988.
(9) Lee, M. M.; Teuscher, J.; Miyasaka, T.; Murakami, T. N.; Snaith, H. J. Efficient Hybrid Solar Cells Based on Meso-Superstructured Organometal Halide Perovskites. *Science* **2012**, *338*, 643−647.
(10) http://www.nrel.gov/ncpv/images/efficiency_chart.jpg, The National Renewable Energy Laboratory (NREL); 2015.
(11) Noel, N. K.; Stranks, S. D.; Abate, A.; Wehrenfennig, C.; Guarnera, S.; Haghighirad, A.; Sadhanala, A.; Eperon, G. E.; Pathak, S. K.; Johnston, M. B.; Petrozza, A.; Herz, L.; Snaith, H. Lead-Free

DOI: 10.1021/acsami.5b05104
ACS Appl. Mater. Interfaces 2015, 7, 17482−17488

Organic-Inorganic Tin Halide Perovskites for Photovoltaic Applications. *Energy Environ. Sci.* **2014**, *7*, 3061−3068.
(12) Noh, J. H.; Im, S. H.; Heo, J. H.; Mandal, T. N.; Seok, S. I. Chemical Management for Colorful, Efficient, and Stable Inorganic-Organic Hybrid Nanostructured Solar Cells. *Nano Lett.* **2013**, *13*, 1764−1769.
(13) Chen, H.; Pan, X.; Liu, W.; Cai, M.; Kou, D.; Huo, Z.; Fang, X.; Dai, S. Efficient Panchromatic Inorganic-Organic Heterojunction Solar Cells with Consecutive Charge Transport Tunnels in Hole Transport Material. *Chem. Commun.* **2013**, *49*, 7277−7179.
(14) Xiao, Y. M.; Han, G. Y.; Chang, Y. Z.; Zhou, H. H.; Li, M. Y.; Li, Y. P. An All-solid-state Perovskite-Sensitized Solar Cell Based on the Dual Function Polyaniline as the Sensitizer and p-Type Hole-Transporting Material. *J. Power Sources* **2014**, *267*, 1−8.
(15) Qin, P.; Tanaka, S.; Ito, S.; Tetreault, N.; Manabe, K.; Nishino, H.; Nazeeruddin, M. K.; Gratzel, M. Inorganic Hole Conductor-Based Lead Halide Perovskite Solar Cells with 12.4% Conversion Efficiency. *Nat. Commun.* **2014**, *5* (3834), 1−6.
(16) Christians, J. A.; Fung, R. C.; Kamat, P. V. An Inorganic Hole Conductor for Organo-Lead Halide Perovskite Solar Cells. Improved Hole Conductivity with Copper Iodide. *J. Am. Chem. Soc.* **2014**, *136*, 758−764.
(17) Hu, L.; Wang, W.; Liu, H.; Peng, J.; Cao, H.; Shao, G.; Xia, Z.; Ma, W.; Tang, J. PbS Colloidal Quantum Dots as an Effective Hole Transporter for Planar Heterojunction Perovskite Solar Cells. *J. Mater. Chem. A* **2015**, *3*, 515−518.
(18) Etgar, L.; Grätzel, M.; Gao, P.; Qin, P.; Nazeeruddin, M. K. Hybrid Lead Iodide Perovskite and Lead Sulfide QDs Heterojunction Solar Cell to Obtain Panchromatic Response. *J. Mater. Chem. A* **2014**, *2*, 11586−11590.
(19) Seo, G.; Seo, J.; Ryu, S.; Yin, W.; Ahn, T. K.; Seok, S. I. Enhancing the Performance of Sensitized Solar Cells with PbS/$CH_3NH_3PbI_3$ Core/Shell Quantum Dots. *J. Phys. Chem. Lett.* **2014**, *5*, 2015−2020.
(20) Jara, D. H.; Yoon, S. J.; Stamplecoskie, K. G.; Kamat, P. V. Size-Dependent Photovoltaic Performance of $CuInS_2$ Quantum Dot-Sensitized Solar Cells. *Chem. Mater.* **2014**, *26*, 7221−7228.
(21) Yu, W. W.; Qu, L. H.; Guo, W. Z.; Peng, X. G. Experimental Determination of the Extinction Coefficient of CdTe, CdSe, and CdS Nanocrystals. *Chem. Mater.* **2003**, *15*, 2854−2860.
(22) Tisdale, W. A.; Williams, K. J.; Timp, B. A.; Norris, D. J.; Aydil, E. S.; Zhu, X. Y. Hot-Electron Transfer from Semiconductor Nanocrystals. *Science* **2010**, *328*, 1543−1547.
(23) Semonin, O. E.; Luther, J. M.; Choi, S.; Chen, H. Y.; Gao, J. B.; Nozik, A. J.; Beard, M. C. Peak External Photocurrent Quantum Efficiency Exceeding 100% via MEG in a Quantum Dot Solar Cell. *Science* **2011**, *334*, 1530−1533.
(24) Kolny-Olesiak, J.; Weller, H. Synthesis and Application of Colloidal $CuInS_2$ Semiconductor Nanocrystals. *ACS Appl. Mater. Interfaces* **2013**, *5*, 12221−12237.
(25) Tell, B.; Shay, J. L.; Kasper, H. M. Electrical Properties, Optical Properties, and Band Structure of $CuGaS_2$ and $CuInS_2$. *Phys. Rev. B* **1971**, *4*, 2463−2471.
(26) Zhou, Z. J.; Yuan, S. J.; Fan, J. Q.; Hou, Z. L.; Zhou, W. H.; Du, Z. L.; Wu, S. X. $CuInS_2$ Quantum Dot-Sensitized TiO_2 Nanorod Array Photoelectrodes: Synthesis and Performance Optimization. *Nanoscale Res. Lett.* **2012**, *7* (652), 1−8.
(27) Pan, Z. X.; Mora-Sero, I.; Shen, Q.; Zhang, H.; Li, Y.; Zhao, K.; Wang, J.; Zhong, X. H.; Bisquert, J. High-Efficiency "Green" Quantum Dot Solar Cells. *J. Am. Chem. Soc.* **2014**, *136*, 9203−9210.
(28) Look, D. C.; Manthuruthil, J. C. Electron and Hole Conductivity in $CuInS_2$. *J. Phys. Chem. Solids* **1976**, *37*, 173−180.
(29) Tiwari, A. N.; Pandya, D. K.; Chopra, K. L. Electrical and Optical-Properties of Single-Phase $CuInS_2$ Films Prepared Using Spray Pyrolysis. *Thin Solid Films* **1985**, *130*, 217−230.
(30) Watanabe, T.; Nakazawa, H.; Matsui, M. Improvement of the Electrical Properties of Cu-poor $CuInS_2$ Thin Films by Sodium Incorporation. *Jpn. J. Appl. Phys.* **1998**, *37*, L1370−L1372.
(31) Ellingson, R. J.; Beard, M. C.; Johnson, J. C.; Yu, P. R.; Micic, O. I.; Nozik, A. J.; Shabaev, A.; Efros, A. L. Highly Efficient Multiple Exciton Generation in Colloidal PbSe and PbS Quantum Dots. *Nano Lett.* **2005**, *5*, 865−871.
(32) Murray, C. B.; Norris, D. J.; Bawendi, M. G. Synthesis and Characterization of Nearly Monodisperse Cde (E = S, Se, Te) Semiconductor Nanocrystallites. *J. Am. Chem. Soc.* **1993**, *115*, 8706−8715.
(33) Li, L.; Pandey, A.; Werder, D. J.; Khanal, B. P.; Pietryga, J. M.; Klimov, V. I. Efficient Synthesis of Highly Luminescent Copper Indium Sulfide-Based Core/Shell Nanocrystals with Surprisingly Long-Lived Emission. *J. Am. Chem. Soc.* **2011**, *133*, 1176−1179.
(34) Castro, S. L.; Bailey, S. G.; Raffaelle, R. P.; Banger, K. K.; Hepp, A. F. Synthesis and Characterization of Colloidal $CuInS_2$ Nanoparticles from a Molecular Single-Source Precursor. *J. Phys. Chem. B* **2004**, *108*, 12429−12435.
(35) Son, D. H.; Hughes, S. M.; Yin, Y. D.; Alivisatos, A. P. Cation Exchange Reactions in Ionic Nanocrystals. *Science* **2005**, *36*, 1009−1012.
(36) Burschka, J.; Pellet, N.; Moon, S. J.; Humphry-Baker, R.; Gao, P.; Nazeeruddin, M. K.; Gratzel, M. Sequential Deposition as a Route to High-Performance Perovskite-Sensitized Solar Cells. *Nature* **2013**, *499*, 316−319.
(37) Heo, J. H.; Im, S. H.; Noh, J. H.; Mandal, T. N.; Lim, C.-S.; Chang, J. A.; Lee, Y. H.; Kim, H. J.; Sarkar, A.; Nazeeruddin, M. K. Efficient Inorganic−Organic Hybrid Heterojunction Solar Cells Containing Perovskite Compound and Polymeric Hole Conductors. *Nat. Photonics* **2013**, *7*, 486−491.
(38) Wu, Y. Z.; Yang, X. D.; Chen, H.; Zhang, K.; Qin, C. J.; Liu, J.; Peng, W. Q.; Islam, A.; Bi, E. B.; Ye, F.; Yin, M. S.; Zhang, P.; Han, L. Y. Highly Compact TiO_2 Layer for Efficient Hole-Blocking in Perovskite Solar Cells. *Appl. Phys. Express* **2014**, *7*, 052301.
(39) Peng, B.; Jungmann, G.; Jager, C.; Haarer, D.; Schmidt, H. W.; Thelakkat, M. Systematic Investigation of the Role of Compact TiO_2 Layer in Solid State Dye-Sensitized TiO_2 Solar Cells. *Coord. Chem. Rev.* **2004**, *248*, 1479−1489.
(40) Santra, P. K.; Nair, P. V.; George Thomas, K.; Kamat, P. V. $CuInS_2$-Sensitized Quantum Dot Solar Cell. Electrophoretic Deposition, Excited-State Dynamics, and Photovoltaic Performance. *J. Phys. Chem. Lett.* **2013**, *4*, 722−729.
(41) Im, J. H.; Jang, I. H.; Pellet, N.; Gratzel, M.; Park, N. G. Growth of $CH_3NH_3PbI_3$ Cuboids with Controlled Size for High-Efficiency Perovskite Solar Cells. *Nat. Nanotechnol.* **2014**, *9*, 927−932.
(42) Kim, H. S.; Lee, J. W.; Yantara, N.; Boix, P. P.; Kulkarni, S. A.; Mhaisalkar, S.; Gratzel, M.; Park, N. G. High Efficiency Solid-State Sensitized Solar Cell-Based on Submicrometer Rutile TiO_2 Nanorod and $CH_3NH_3PbI_3$ Perovskite Sensitizer. *Nano Lett.* **2013**, *13*, 2412−2417.
(43) Kim, H. S.; Mora-Sero, I.; Gonzalez-Pedro, V.; Fabregat-Santiago, F.; Juarez-Perez, E. J.; Park, N. G.; Bisquert, J. Mechanism of Carrier Accumulation in Perovskite Thin-Absorber Solar Cells. *Nat. Commun.* **2013**, *4* (2242), 1−7.
(44) Dualeh, A.; Tétreault, N.; Moehl, T.; Gao, P.; Nazeeruddin, M. K.; Grätzel, M. Effect of Annealing Temperature on Film Morphology of Organic-Inorganic Hybrid Pervoskite Solid-State Solar Cells. *Adv. Funct. Mater.* **2014**, *24*, 3250−3258.
(45) Mora-Sero, I.; Bisquert, J.; Fabregat-Santiago, F.; Garcia-Belmonte, G.; Zoppi, G.; Durose, K.; Proskuryakov, Y.; Oja, I.; Belaidi, A.; Dittrich, T.; Tena-Zaera, R.; Katty, A.; Levy-Clement, C.; Barrioz, V.; Irvine, S. J. C. Implications of the Negative Capacitance Observed at Forward Bias in Nanocomposite and Polycrystalline Solar Cells. *Nano Lett.* **2006**, *6*, 640−650.
(46) Chavhan, S.; Miguel, O.; Grande, H. J.; Gonzalez-Pedro, V.; Sanchez, R. S.; Barea, E. M.; Mora-Sero, I.; Tena-Zaera, R. Organo-metal Halide Perovskite-Based Solar Cells with CuSCN as the Inorganic Hole Selective Contact. *J. Mater. Chem. A* **2014**, *2*, 12754−12760.

DOI: 10.1021/acsami.5b05104
ACS Appl. Mater. Interfaces 2015, 7, 17482−17488

(47) Liu, D. Y.; Yang, J. L.; Kelly, T. L. Compact Layer Free Perovskite Solar Cells with 13.5% Efficiency. *J. Am. Chem. Soc.* **2014**, *136*, 17116−17122.
(48) Guillén, E.; Ramos, F. J.; Anta, J. A.; Ahmad, S. Elucidating Transport-Recombination Mechanisms in Perovskite Solar Cells by Small-Perturbation Techniques. *J. Phys. Chem. C* **2014**, *118*, 22913−22922.

DOI: 10.1021/acsami.5b05104
ACS Appl. Mater. Interfaces 2015, 7, 17482−17488